Revue des Composites et des Matériaux Avancés-Journal of Composite and Advanced Materials
Vol. 35, No. 3, June, 2025, pp. 529-542
Journal homepage: http://iieta.org/journals/rcma

Investigating Quantum Chemical Properties of Polymeric Fillers D1 Phenyl-P and D2 10-MDP via Gaussian 90 and DFT

Sarah M. Hameed*, Sahib N. Abdul-wahid

Department of Physics, College of Education for Girls, Kufa University, Najaf 54001, Iraq

Corresponding Author Email: sarahmajidhameed@gmail.com

https://doi.org/10.18280/rcma.350314

Received: 17 October 2024
Revised: 20 December 2024
Accepted: 2 January 2025
Available online: 30 June 2025

Keywords:
density functional theory (DFT), polymeric dental fillers, electronic structure, spectroscopic analysis, UV absorption, dental applications

ABSTRACT

The study compares the characteristics of D1 Phenyl-P and D2 10-MDP using density functional theory (DFT) with the B3LYP functional and the G3-21 basis set for quantum chemical computations. The Gaussian 90 program was used to design the molecular formulation for the studied polymeric dental fillers, and DFT. The hybrid function B3LYP was also adopted to process the calculations for molecules, and the data of basis set G 3-21 was used to calculate quantum electronic properties such as energies. D1 Phenyl-P has a greater ionization potential and electron affinity, implying more stability in keeping electrons, but D2 10-MDP has a higher electronic chemical potential, making it more reactive. D1 Phenyl-P has a higher chemical hardness, which makes it more resistant to deformation, whereas D2 is softer and more reactive. The spectral features show that D2 10-MDP is more active in the infrared and Raman spectra, with greater P=O and P-O-C vibrations, which represent its adhesive qualities. Furthermore, D2 10-MDP exhibits greater UV absorption in the 80–100 nm region than D1 Phenyl-P, which is why it is more useful for UV-curable applications. By understanding the molecular characteristics of D1 Phenyl-P and D2 10-MDP through DFT analysis, this study provides valuable data to design high-performance dental adhesives and materials. D2 10-MDP emerges as a superior candidate for adhesives requiring high reactivity and UV-curability, while D1 Phenyl-P offers enhanced stability for structural applications. Together, these insights drive innovation in adhesive dentistry, ensuring better clinical outcomes and patient satisfaction.

1. INTRODUCTION

A laser is a certain type of electromagnetic radiation that gives out energy and has its own distinct qualities. LASER stands for "light amplifier for stimulated emission." An apparatus that produces coherent electromagnetic radiation is a laser. With few exceptions, a well-defined wavelength and minimal ramification of the radiance beam distinguish laser radiance [1-3]. The most important factor in determining how light affects tissue is wavelength. This is the separation of two successive wave peaks. Various laser types have different wavelengths based on the sort of active medium they use. The length of a laser wavelength is commonly expressed in micrometers or (microns) nanometers (nm), depending on whether the wavelength falls within the electromagnetic spectrum's ultraviolet, visible, or infrared regions. In other words, the wavelength dictates the quality [4]. Lasers have become integral to modern dentistry, offering precise and minimally invasive treatments for both hard and soft tissues. In hard tissue procedures, lasers assist in detecting cavities, preparing teeth for fillings—often reducing the need for anesthesia—and sealing tubules to alleviate tooth sensitivity. For soft tissue applications, lasers enable reshaping gum tissue to correct gummy smiles, performing frenectomies, and removing benign tumors with minimal discomfort and faster healing. Additionally, lasers enhance teeth whitening processes and aid in managing conditions like sleep apnea by reshaping throat tissues. Their ability to reduce pain and accelerate healing makes lasers a valuable tool in various dental treatments [5].

Dental caries is a significant issue for world health [6]. They build a progressive viral illness that eventually results in cavities by demineralizing and destroying the organic component of tooth tissues by the enzyme proteolytic degradation [7]. Acid is produced and minerals are lost from enamel and dentine as a result of dental bacteria' metabolic processes when they consume carbohydrates in the plaque biofilm [8].

There are numerous techniques accessible for excavating caries [9]. Employing a rotating bur is a typical approach. This is a highly efficient and inexpensive method, but it produces a lot of noise and vibration. Applying an erbium laser beam is another strategy. This is a relatively new technique, and most nations have not yet adopted it widely. Water molecules in the dental hard tissues absorb light from the laser beam when it impacts the tooth surface. The water quickly heats up and vaporizes as a result [10]. Dental hard tissue is ablated as an

outcome of the reaction, which also generates a micro-explosion and high localized pressure. An extensive paper has been produced that covers the basic concepts and broad utilization of lasers in dentistry [11].

When preparing cavities during dental treatment, the laser system affords a number of benefits over conventional procedures involving mechanical drill. Laser-based techniques may be used for tooth cavity preparation, dentin diagnostic, and treatment. Today a laser is an essential instrument for a lot of contemporary treatments. A variety of laser beams that have different pulse lengths and durations over a range of wavelengths have been used in previous research on the destruction of human hard structure or mass [12].

This laser may be useful since the carbon dioxide laser stimulation wavelengths that are well absorbed in tissues fall between 9.3 and 10.6 μm. By employing different pulse lengths, it has been found that the laser can cleave dentine and enamel tissues without producing any heat stress; however, this is only possible when the laser interacts with a water spray [13]. At the same time, the most effective ablation can be achieved with longer pulses. With a low pulse repetition rate and a pulse length of, this laser could cut dentine and enamel without damaging tissue structure or producing heat damage. However, dentine injury was observed during the use of pulses. Small pulse repetition amounts were used to remove rotting dentine without carbonizing the tissues around it by using laser pulses without concurrently. spraying water. But the effects on enamel were not examined, and hard dentine was not ablated very well. The varying tissue reactions and removal rates for different lasers demonstrate how the energy density, repetition, and length of the laser pulses impact how the laser interactions with tissue; similar [14].

Theoretical computations in physics and chemistry are often applied when a mathematical approach is sufficiently developed and can be efficiently conducted utilizing computer methods [15].

The analysis of developments having chemical relevance is accomplished in theoretical chemistry and physics by combining mathematical techniques with the basic laws of physics. Molecular modeling, another name for computational chemistry, is a fundamental and significant technique employed in molecular science studies [16].

In physics, molecular modeling approaches are being used more and more to quantitatively study a wide range of features, including as molecular energies, geometries, electronic structures, electron and charge distributions, and infrared (IR) and ultraviolet (UV) light, and other physical characteristics. These techniques are applied to a diverse range of molecular systems, including inorganic, biological, polymeric, organometallic, catalytic, pharmaceutical, and various other domains [17].

In computational chemistry and physics, there are four main methods that are often used: semi-empirical methods (SE), density functional theory (DFT), ab initio methods, and molecular mechanics. Molecular quantum mechanics is the most important part of theoretical physics [18]. Over the past three decades, DFT has demonstrated significant success in identifying organometallic ratios, yielding reliable structural and energetic predictions with moderate computational cost. As a result, it has become the most popular way to do theoretical investigations and assessments of molecular systems [19].

In this study, we looked into the quantum electronic properties of two polymers, D1 Phenyl-P and D2 10-MDP. We focused on key factors like electron affinity, chemical hardness potential, chemical softness, and electronegativity. We also examined their spectral properties, including the infrared (IR) absorption spectra of both the HEMA (D1) polymer and HEMA phosphate (D2), along with the Raman spectra. Finally, we explored the optical properties of both polymers, specifically their absorption and conductivity, to better understand their behavior.

2. COMPUTATIONAL METHODS

The Gaussian 90 program was used to design the molecular formulation for the studied polymeric dental fillers, and the theory of density functional (DFT) [20]. The Gaussian 90 program is a cornerstone in computational chemistry, used to perform quantum chemical calculations on molecular systems. It employs various computational methods to solve the Schrödinger equation for molecular systems, focusing on both wave function-based and density-based approaches. Density functional theory (DFT) is a quantum mechanical technique that concentrates on the electron density ($\rho(r)$ rather than the many-electron wave function. DFT simplifies the problem of electron-electron interactions, making it computationally efficient for studying large molecular and condensed matter systems. The program's characteristics were used to perform geometric optimization on the lengths and angles of the molecular bonds. The hybrid function B3LYP was also adopted to process the calculations for molecules, and a basis set G 3-21 was used to calculate quantum electronic properties such as energies. Molecular orbitals HOMO and LOMO, occupied gap energy (Egap), and quantum chemical properties such as ionization potential, chemical hardness, chemical softness, chemical potential, etc.

In this study, we calculated the spectral characteristics, such as the infrared and Raman spectra, for each of the filler molecules we looked at. We then simulated the photon generation of laser beams by modeling the time-ratio equations in a four-level CO_2 laser system using the Runge-Kutta method, with the equations programmed in MATLAB 2021. We figured out the density distribution of the energy levels (N1, N2, N3, and N4) and how strong the laser beam was. To put the results into a practical context, we simulated the drilling of a human tooth using the generated CO_2 laser and tracked how the mass and depth changed over time due to the drilling process.

3. RESULTS AND DISCUSSIONS

3.1 Laser properties of CO_2 by MATLAB processing

MathWorks, Inc. established MATLAB®, a software programming for numerical calculation, simulation, and visualization of the chemical structures. It is frequently employed in research, education, and business to address both general and application-specific issues that come up in a variety of fields. MATLAB provides several collections of application-specific scripts, referred known as "toolboxes," for this purpose. A Laser Toolbox is presented, containing many scripts for laser material contact and process modeling, as well as analysis and visualization of laser beam parameters. The author's website has the documentation, examples, and tools. The Laser Toolbox may be used on any MATLAB-supported

operating system and was created for MATLAB version 9.10.0 (R2021a).

During the main discharge the molecules were formed to the original gas blend of the regime The equation expressing the energy within the vibrational modes of CO_2 and the vibrational N2 and CO_2 can be found. The studies [21-23] solving the rate equations for the regime using a MATLAB method that is based on the Rung-Kutta method [24]. The data related to the equations and the reference [25] showed the output laser pulse got in our work.

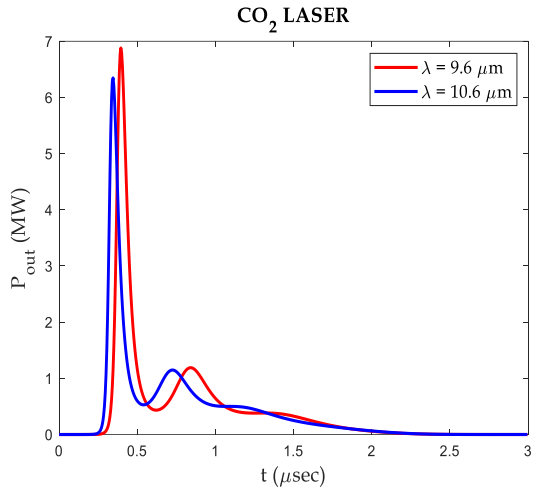

Figure 1. The laser's output power in relation to time [26]

The Figure 1 The graph illustrates the output power of a CO_2 laser over time, showing how different reflectivity levels (80%, 86%, and 90%) of the laser cavity mirrors affect the laser's performance. As reflectivity increases, the laser reaches a higher peak power, with the maximum occurring for 90% reflectivity. The pulse initially spikes sharply and then experiences a damped oscillation as the power decays. Higher reflectivity results in more extended pulses and more pronounced oscillations, demonstrating that mirror reflectivity significantly impacts both the peak power and the pulse duration in pulsed laser systems.

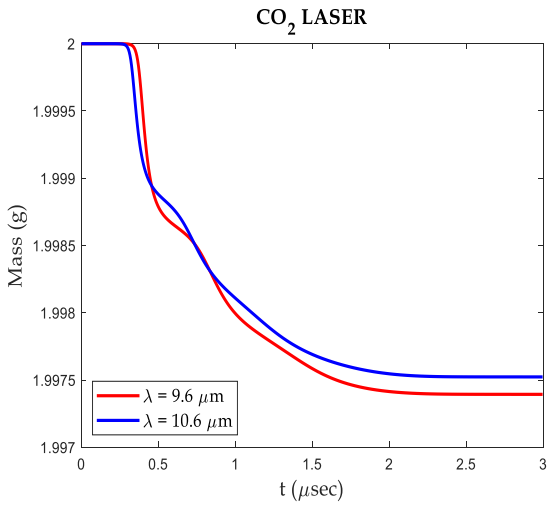

Figure 2. Tooth loss in mass with time [26]

The Figure 2 shows the mass loss of a sample, likely teeth, over time when exposed to a CO_2 laser at wavelengths of 9.6 µm and 10.6 µm. Both wavelengths cause a rapid initial decrease in mass due to material ablation, with the 9.6 µm wavelength leading to a slightly greater mass loss. After the initial sharp decline, the mass stabilizes, indicating a reduction in the rate of material removal. Overall, the 9.6 µm wavelength appears to be marginally more effective at reducing the mass of the sample compared to the 10.6 µm wavelength.

The Figure 3 shows, over time, the depth of drilling into a sample—likely teeth—when exposed to a CO_2 laser of wavelengths of 9.6 µm and 10.6 µm. Both wavelengths cause a rapid initial increase in depth, with the 9.6 µm wavelength penetrating slightly faster and deeper than the 10.6 µm wavelength. After the initial sharp increase, the depth growth slows and eventually stabilizes, with the final depth being slightly greater for the 9.6 µm wavelength, indicating that it is marginally more effective in achieving deeper penetration.

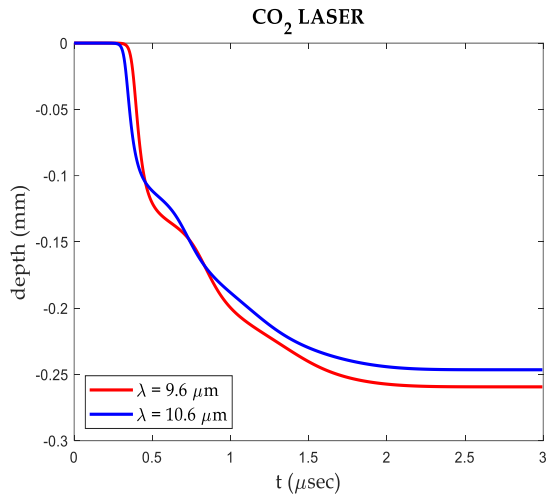

Figure 3. The depth of drilling into teeth over time [26]

3.2 Geometrical structure optimization of Phenyl-P (D1), and 10-MDP (D2)

The optimal atomic configuration for increasing the stability of the molecule was determined by geometry optimization [27]. In this study, we looked at many dental polymers, labeled A and B in Figure 4, to look a chemical structure with the best optoelectronic criteria for use in Phenyl-P (D1) and 10-MDP applications. Getting a molecule's structure just right is crucial for predicting its properties. Before a structure reaches its most stable form (or optimized structure), several steps are required to fine-tune it (Figure 4). To check the accuracy of the optimized structures, we calculated the bond lengths and angles, which helped determine whether they were at a stable state or a transition point. If a structure has higher-order bond lengths and angles, it's considered to be at a transition state. Finally, once a structure reaches its lowest energy state, it should have no negative frequencies, indicating that it's fully optimized.

The density functional theory (DFT) approach using the B3LYP functional and the 6-31G basis set was used for maximizing the molecules Phenyl-P (D1) with 34 atoms and 150 electrons and 10-MDP (D2) with 48 atoms and 174 electrons.

The optimization process of Phenyl-P using the approach of density functional theory (DFT) with the B3LYP functional and the data of 6-31G(d) basis set involves calculating the molecular structure by minimizing the energy of the system while adhering to quantum mechanical principles. The B3LYP

functional is a combination of Becke's three-parameter exchange functional and the Lee-Yang-Parr correlation functional. It strikes a good compromise between speed and accuracy. The 6-31G(d) basis set has polarization functions that contribute to making it easier to describe molecular orbitals in systems where electrons are spread out, such phenyl and phosphate groups. During optimization, the geometry of Phenyl-P is iteratively adjusted until the total energy and forces on atoms converge to a minimum. This ensures that the resulting structure corresponds to the molecule's stable configuration under the applied theoretical conditions. The approach is widely used for studying electronic properties, reactivity, and conformational behavior of molecules.

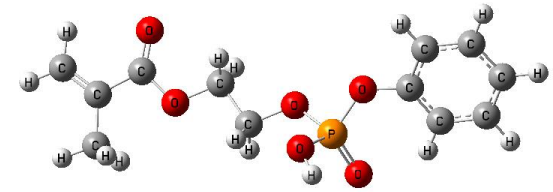

(A) Phenyl-P(D1)

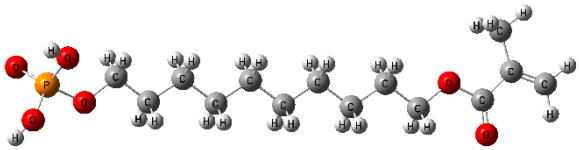

(B) 10-MDP(D2)

Figure 4. Optimizing the geometric structure of (A) D1 Phenyl-P and (B) D2 10-MDP [26]

The optimization of 10-MDP (10-methacryloyloxydecyl dihydrogen phosphate) using the density functional theory (DFT) approach using the B3LYP functioning and 6-31G(d) basis set focuses on understanding the molecule's stable shape with minimal energy. B3LYP combines Becke's hybrid exchange and the Lee-Yang-Parr correlation functioning, providing a better balance of accuracy and computational cost for organic and organophosphorus compounds like 10-MDP. The 6-31G(d) basis set, which includes polarization functions, enhances the description of the electronic environment around the phosphate group and the long hydrocarbon chain. The optimization iteratively adjusts bond lengths, angles, and dihedral angles until energy convergence and force thresholds are met. This ensures the final structure accurately reflects the molecule's equilibrium configuration, capturing both the rigidity of the phosphate group and the flexibility of the methacryloyloxy and decyl moieties. Such calculations are crucial for understanding the molecular interactions and reactivity of 10-MDP in adhesive and biomaterial applications.

Using the DFT approach and the B3LYP functioning in the Gaussian 09 program, we found the geometrical specifications for D1 Phenyl-P and 10-MDP (D2). These are shown in Tables 1 and 2. The bond angles and bond lengths (in angstroms) are compared to previously published results. Once a structure reaches its lowest energy state, it should show no negative frequencies, which means it has been fully optimized.

In Table 1, we compare two dental polymers, D1 (phenyl-P) and D2 (10-MDP), which have different bond lengths that highlight noticeable structural differences. These variations could influence their chemical and physical properties. For example, the similar C=C bond lengths suggest that the double bond properties are alike in both polymers, while the slight difference in C-H bond lengths hints at different electrical environments or the effects of their substituents. D2's longer O-C and O-P bonds than D1's could have an impact on reactivity and electron distribution. Interestingly, D1 has a C=O group that is missing from D2, indicating a difference in functional groups. Furthermore, their capability for hydrogen bonding and interaction with surrounding materials is further distinguished by the presence of an O-H bond in D1 and its absence in D2. Understanding these differences is important for comprehending the behavior of these polymers in dental applications, especially with reference to mechanical strength and moisture sensitivity [28].

Table 1. Lengths of bonds in studied dental polymeric materials (in A°) [26]

Dental Polymeric Materials	Bond Length (A°)	
	D1 Phenyl-P	D2 10-MDP
H– C	1.084	1.092
C = C	1.335	1.335
C– O	1.412	1.490
O – H	0.993	0.993
C – C	1.509	1.524
O – P	1.654	1.670
C = O	1.228	–
P = O	10554	–

Table 2. Angles of bonds in studied dental polymeric materials (in degrees) [26]

Dental Polymeric Materials	Bonds Angle (in Degree)	
	D1 Phenyl-P	D2 10-MDP
H – C – H	118.088	109.664
C – O – C	115.199	115.513
O = C – C	122.235	122.776
O = C = C	--	126.723
C –C= C	116.851	--
C= C – H	119.994	119.883
C – C –O	103.938	106.110
C – O – P	119.765	---
O – P = O	114.629	--
P – O – H	114.152	114.167
P – O – C	172.510	118.645
O – C = C	115.248	--
C= C= C	119.515	--
C– C– C	–	111.436
C –C – H	–	111.936

In Table 2, the comparison of bond angles between D1 (Phenyl-P) and D2 (10-MDP) reveals structural variations reflecting their distinct chemical frameworks. D1 generally exhibits larger bond angles, particularly in P–O–C (172.510°) and O–P=O (114.629°), indicative of more linear arrangements around phosphorus. D2, with smaller angles like C–C–C (111.436°) and C–C–H (111.936°), reflects its aliphatic and flexible nature. Similarities, such as nearly identical angles for P–O–H (114.152° vs. 114.167°) and C=C–H (119.994° vs. 119.883°), show consistent bonding characteristics across shared functional groups. Unique angles, like O=C=C in D2 (126.723°) and C=C=C in D1 (119.515°), emphasize differences due to conjugation and structural features, highlighting their specialized roles in dental polymer applications.

3.3 Quantum electronic properties of D1 Phenyl-P, and D2 10 MDP Dental polymers

HOMO (Highest Occupied Molecular Orbital): The HOMO is the molecular orbital in a molecule that contains the highest energy electrons among all the occupied orbitals. LUMO (Lowest Unoccupied Molecular Orbital): The LUMO is the lowest-energy molecular orbital that is unoccupied by electrons in a molecule. It represents the first orbital that can accept electrons during a reaction.

We were able to learn about the similarity of electron states and transported electrons by using the HOMO and LUMO orbits [28].

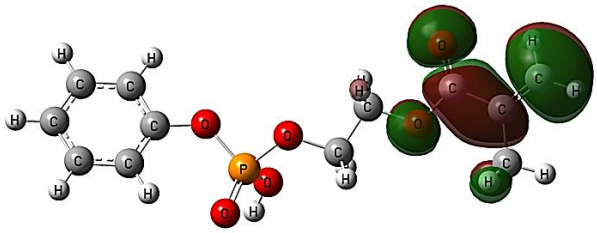

(A) LUMO D1 Phenyl-P

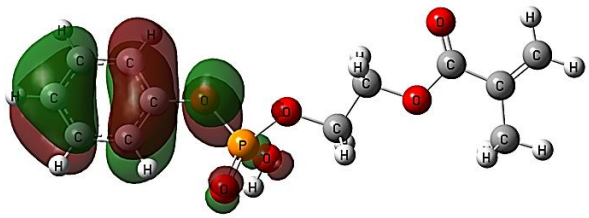

(A) HOMO D1 Phenyl-P

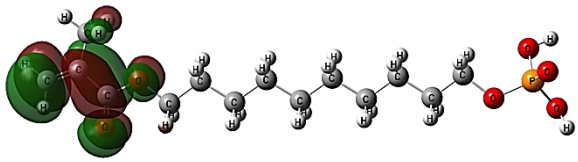

(B) LUMO D2 10 MDP

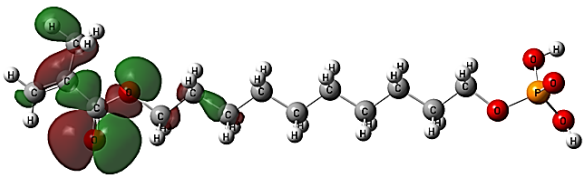

(B) HOMO D2 10-MDP

Figure 5. The molecular orbitals LUMO and HOMO of (A) D1 Phenyl-P and (B) D2 10-MDP [26]

Figure 5 shows the molecular orbitals, HOMO and LUMO, for (A) D1 Phenyl-P and (B) D2 10-MDP.

Based on Table 3, observe that the HOMO energies decline in the following order: D2<D1, while the LUMO energies for D2>D1. This demonstrates that the considerable influence of the terminal electron donor on the examined compound's HOMO affects the order relative to the energy gap. This shows that there is a great effect on the ability to donate electrons for D2, while it is less than in D1, while D1 has a higher homo energy than D2, and this gives it the advantage of not being able to donate electrons or reach the excited state [30].

Additionally, we point out that D1 has a smaller gap than the other dental polymer (D2) under study due to its high HOMO energy. Therefore, unlike the D2, this dental polymer is not too occupied, possibly due to the more substantial terminal donor and higher conjugation between the donors and conjugated -system [30].

Table 3. Gap energies and molecular orbitals of the studied dental polymeric materials

Dental Polymeric Materials	in (eV)			
	E_{Total} (eV)	E_{HOMO} (eV)	E_{LUMO} (eV)	E_{gap} (eV)
Phenyl-P	-34239.862	-6.407	-2.470	3.993
10-MDP	-36505.341	-6.210	-2.220	3.990

According to Koopman's theorem, the band gap is defined by the energy difference between the highest occupied molecular orbital (HOMO) and the lowest unoccupied molecular orbital (LUMO). Table 3 presents the energy gaps for D1 Phenyl-P and 10-MDP, indicating that these polymers exhibit insulating and non-conductive properties across the energy gap. The energy gaps are illustrated in Figure 6 for (a) Phenyl-P and (b) 10-MDP.

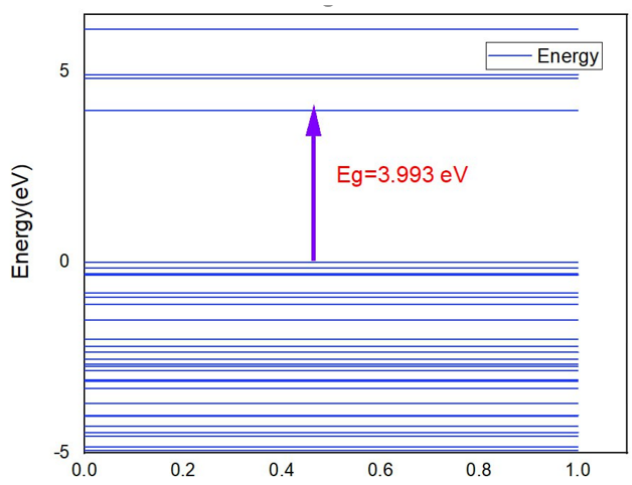

(a) Phenyl-P

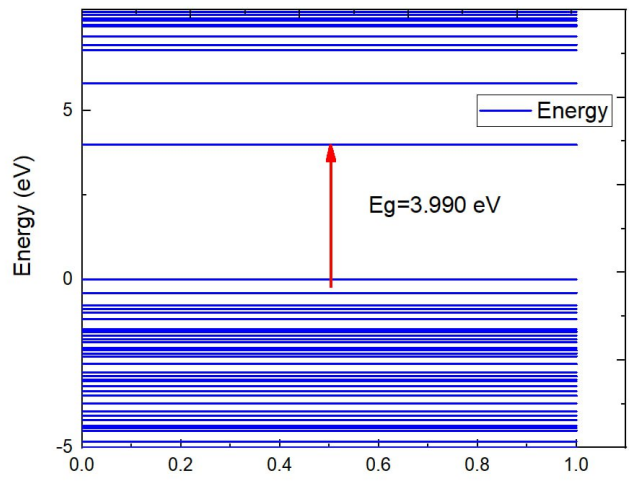

(b) 10-MDP

Figure 6. the energy gap for (a) Phenyl-P, and (b)10-MDP [26]

Table 4. Electronic characteristics of the dental polymeric materials under investigation

Dental Polymeric Materials	I_p (eV)	E_A (eV)	(eV)	(eV)	S (eV^{-1})	(eV)	(eV)
D1 Phenyl-P	6.463	2.470	1.996	-4.467	0.250	4.997	4.467
D2 10-MDP	6.210	2.220	1.995	-4.215	0.251	4.453	4.215

Figure 7 shown the charge density distribution of D2 10 MDP and D1 Phenyl-P. The ionization potential (IP) of a molecule is the amount of energy needed for removing an electron from that molecule or isolated atom. It can be defined as the energy differential between the positive charged energy E (+) and the neutral energy E(n) based on the connection that follow [31] and the value of the ionization potential of D1 6.463 (eV) and, D2 is 6.210 (eV).

$$\mathbf{Ip\ (eV)} = E_{(+)} - E_{(n)} = -E_{HOMO} \tag{1}$$

As a result, the ionization potential of polymer D1 is substantially larger than that of polymer D2, suggesting that D1 has a lesser inclination to undergo ionization.

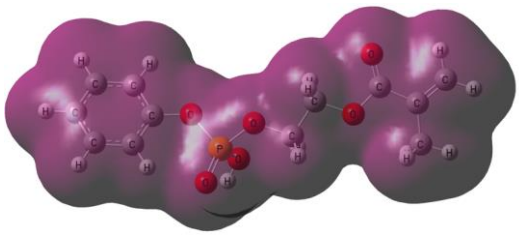

(a) Phenyl-P(D1)

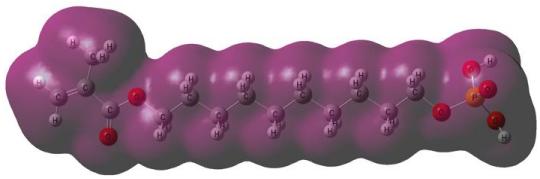

(b) 10 MDP(D2)

Figure 7. Charge density distribution of (a) D1 Phenyl-P, and (b) D2 10 MDP [26]

When a neutral atom gains an electron to form a negative ion, the energy difference between the neutral state $D(n)$ and the negatively charged state $E(-)$ can be described by the following equation. This energy difference is known as the electron affinity (EA) [32]:

$$\text{EA (eV)} = E_{(n)} - E_{(-)} = -E_{LUMO} \tag{2}$$

Referring to Table 4, it is evident that D1 has a higher electron affinity than D2. This indicates that the D1 molecule has a stronger capacity to attract electrons.

Chemical potential (μ): The electronic chemical potential is a fundamental concept in the variational theory of DFT. It links the reactivity of a molecule to how its electronic energy E changes with variations in external potential and electron count. N. Parr and others have proposed that every system, including both electrons and nuclei, possesses an electrochemical potential. The electronic chemical potential, denoted by μ, is described as follows [33]:

$$\mu\ \text{(eV)} = \left[\frac{\partial E}{\partial N}\right]_V \tag{3}$$

where, v is the nuclei's potential.

Table 4 demonstrates how D1 has an even higher electrical chemical potential than D2. This proves that the D1 molecule possesses a higher external reactivity potential.

Chemical hardness (η) quantifies the degree to which a system resists charge transfer. In the framework of a constant external potential (V), it is characterized in density functional theory as the second derivative of the electronic energy relative to the electron count (N) [34].

$$\eta\ (eV) = \frac{1}{2}\left[\frac{\partial^2 E}{\partial N^2}\right]_V \tag{4}$$

Chemical hardness demonstrates that polymer D1 has a little bit more potential than polymer D2, which means that D1 is better at stopping charge transfer.

$$\eta = \frac{IP - EA}{2} \tag{5}$$

Chemical softness (S) refers to a molecule's level of chemical reactivity. It's essentially the opposite of chemical hardness, with softer molecules being more reactive. (η) [35]:

$$\text{S (eV}-1) = \frac{1}{2\eta} = \left[\frac{\partial N}{\partial \mu}\right]_V \tag{6}$$

The polymer D2 is a little softer than the polymer D1, which means it is more likely to react with chemicals.

Under the designation φ, the tendency of an atom to attract electrons can be conceptualized as the inverse of the electronic chemical potential, a notion that aligns with Pauling's description of electronegativity as "the propensity of an atom within a molecule to draw electrons towards itself" [36].

$$\chi\ \text{(eV)} = -K = -\left[\frac{\partial E}{\partial N}\right]_V \tag{7}$$

By definition, Electrophilicity is an index that measures how stable the energy is when the device picks up more charge from the environment [30]. The measurement of the energy loss caused by a maximum quantity of electron transport between the acceptor and donor is another way to define it [34].

$$\omega\ \text{(eV)} = \frac{K^2}{2\eta} \tag{8}$$

The polymer D1 has a higher electronegativity than the polymer D2, which shows that an atom in a molecule has a higher ability to attract electrons to itself.

Through the calculations listed in the table, we notice that D1 Phenyl-P appears to be more electronegative and electrophilic, with a higher ionization potential and electron affinity, making it more effective in electron-accepting roles compared to D2 10-MDP. D2, on the other hand, has slightly lower electronegativity and ionization potential, suggesting it

may be more efficient in electron-donating processes, which could influence its behavior in dental applications.

3.4 Electrostatic field and spectral properties of D1 Phenyl-P and D2 10-MDP dental polymers

Figure 8(a) shows the electrostatic potential map of the molecule, highlighting areas with varying electron densities, which are likely part of a phenyl-phosphorus complex. The phenyl groups appear electron-rich, while the oxygen atoms bonded to the phosphorus atom display highly negative potential regions, indicating a high electron density around them. The phosphorus atom itself is more electron-deficient, likely appearing with a positive potential. rich regions around the oxygen atoms and phenyl rings, and electron-deficient areas near the phosphorus atom, providing insights into the molecule's reactivity [37].

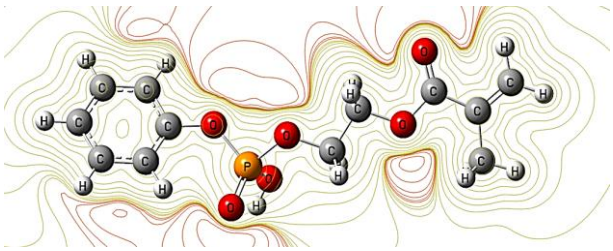

(a) Phenyl-P(D1)

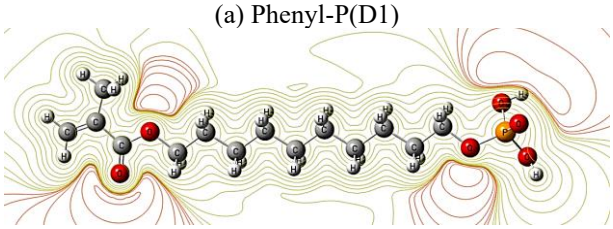

(b) 10 MDP(D2)

Figure 8. Electrostatic field distribution of (a) D1 Phenyl-P, and (b) D2 10 MDP [26]

The electrostatic potential map of Phenyl-P provides a visual representation of the distribution of electrostatic potential across the molecule's surface. This type of map is a critical tool for understanding the electronic structure and reactivity of the molecule. Key features of such a map include regions of positive and negative potential, which correspond to electron-poor and electron-rich areas, respectively.

Key Features of the Map:

1. **Electron-Rich Regions (Negative Potential):**
   - The oxygen atoms of the phosphate group (P=O and P-O bonds) exhibit strong negative potential, appearing as red zones on the map. These regions are electron-rich due to the high electronegativity of oxygen and the resonance stabilization in the phosphate group.
   - The oxygen atoms connected to phenyl and other substituents are also negatively charged, contributing to their ability to act as hydrogen bond acceptors or participate in other interactions.
2. **Electron-Poor Regions (Positive Potential):**
   - The phosphorus atom in the phosphate group shows a positive potential (yellow to light green in the map), reflecting its electron deficiency caused by the withdrawal of electron density by the surrounding oxygen atoms.
   - Hydrogen atoms bonded to carbon in the aromatic phenyl group and the alkyl chain also exhibit slight positive potential (light green to yellow), which makes them less reactive but capable of weak interactions.
3. **Neutral Regions:**
   - The aromatic phenyl ring, despite its electron delocalization, typically shows a relatively neutral potential (green zones), with minor variations depending on the substituents and their electron-withdrawing or -donating effects.

While the Figure 8(b) illustrates the electrostatic potential map of 10-MDP (10-Methacryloyloxydecyl dihydrogen phosphate) reveals key functional regions within the molecule. The phosphate group exhibits high electron density, making it highly negative and ideal for bonding interactions, particularly in dental applications where it binds with calcium in tooth enamel. The central alkyl chain is non-polar, showing uniform low electrostatic potential, which contributes to the molecule's hydrophobicity and flexibility. The methacrylate group has moderate electron density, indicating its reactivity in polymerization processes, crucial for forming strong adhesive bonds. This distribution highlights the molecule's effectiveness in both adhesion and structural integrity in dental materials [38].

The electrostatic potential (ESP) map of 10-MDP (10-methacryloyloxydecyl dihydrogen phosphate) provides critical insights into the electronic distribution and the molecule's potential interactions with other chemical entities. By examining the visual features of the map, we can identify electron-rich and electron-poor regions, which directly impact the molecule’s reactivity and behavior in chemical and biological systems.

Key Features of the ESP Map:

1. **Phosphate Group:**
   - The **phosphate group** (P=O and P-OH bonds) is the most prominent feature with strong **negative electrostatic potential** shown in red. This region is highly electron-rich due to the high electronegativity of oxygen atoms and resonance effects within the phosphate group.
   - The phosphorus atom, surrounded by these highly electronegative oxygen atoms, shows **positive electrostatic potential** (yellow to light green), highlighting its role as an electrophilic center. This makes the phosphate group reactive in nucleophilic attacks or capable of forming ionic bonds.
2. **Methacrylate Group:**
   - The methacrylate moiety displays a distribution of moderate **negative potential** around the carbonyl oxygen atom, shown as red or orange. This indicates its role in hydrogen bonding and reactivity towards nucleophiles.
   - The alkenic carbons in the methacrylate chain show **neutral to slightly positive potential** (green), which may participate in π-π bonding or weak Van der Waals interactions.
3. **Decyl Chain:**
   - The decyl chain, comprising saturated hydrocarbon units, exhibits mostly **neutral potential** (green). This indicates a low likelihood of direct chemical interaction. However, its

hydrophobic nature can play a significant role in nonpolar interactions and self-assembly processes.
- Minor variations in potential can be observed around hydrogen atoms attached to carbons near electronegative groups (e.g., the methacrylate group).

4. **Transition Zones:**
   - The regions between the phosphate group and the hydrocarbon chain exhibit gradients in electrostatic potential. These gradients are indicative of transition zones where polar and nonpolar regions meet, contributing to amphiphilic behavior. This feature is essential for understanding its functionality in interfaces, such as adhesion to surfaces or interaction with biological membranes.

3.5 The spectral criteria of D1 Phenyl-P, and D2 10 MDP dental polymers

3.5.1 Infrared Spectrum (IR) [26]

The IR spectra of D1 Phenyl-P and D2 10 MDP Dental polymers are shown in Figures 8 and 9. The figures show the density functional theory (DFT) (B3LYP) utilizing the Gaussian 90 program with (6-31Ĝ) basis sets.

As shown in Figure 9, the IR spectrum of D1 Phenyl-P reveal identification of Main Peaks:

1. **Broad Peaks Around 3000–3500 cm^{-1} (O-H or N-H Stretching):**
   - If the molecule contains hydroxyl (–OH) or amine (–NH) groups, these peaks indicate hydrogen-bonded stretching vibrations.
   - For 10-MDP or Phenyl-P, this corresponds to the hydroxyl group (P-OH) in the phosphate.
2. **Sharp Peaks Near 2900–3000 cm^{-1} (C-H Stretching):**
   - These peaks correspond to the stretching vibrations of C-H bonds in alkanes and aromatic hydrocarbons.
   - In 10-MDP, these would be associated with the decyl chain and phenyl groups.
3. **Strong Peaks Around 1700–1750 cm^{-1} (C=O Stretching):**
   - This peak indicates the stretching vibration of carbonyl (C=O) groups, such as in esters or ketones.
   - For 10-MDP, this would be due to the methacrylate group.
4. **Peaks Around 1100–1300 cm^{-1} (P=O and P-O Stretching):**
   - These correspond to the characteristic vibrations of the phosphate group, including P=O stretching (near 1250 cm^{-1}) and P-O stretching (near 1100 cm^{-1}).
   - For both Phenyl-P and 10-MDP, this is a critical region to confirm the presence of the phosphate group.
5. **Fingerprint Region (500–1500 cm^{-1}):**
   - This region contains numerous peaks due to complex bending and stretching modes of C-C, C-H, and other bonds in the molecule.
   - For aromatic rings (Phenyl-P) or the methacrylate moiety (10-MDP), peaks in this range represent out-of-plane bending and in-plane stretching vibrations.

The IR spectrum of D1 Phenyl-P reveals a complex vibrational profile, particularly in the fingerprint region (400-1500) cm^{-1}, with strong peaks likely corresponding to C-P, P=O, and P-O-C stretches, indicative of phosphorus-containing groups. A smaller peak around 3000 cm^{-1} suggests the presence of aromatic C-H bonds, consistent with the phenyl group in the molecule. This spectrum highlights the rich vibrational modes associated with the phosphorus functional groups and the phenyl ring, providing a detailed molecular signature that can help confirm the structure of D1 Phenyl-P [39].

In Figure 10, the IR spectrum of 10-MDP (10-Methacryloyloxydecyl dihydrogen phosphate) reveals key vibrational peaks**:**

1. **Broad Peaks at 3000–3500 cm^{-1} (O-H or N-H Stretching):**
   - This region typically corresponds to hydroxyl (–OH) or amine (–NH) stretching vibrations. If present, it may indicate hydroxyl groups associated with phosphate or other functional groups. These peaks are usually broad due to hydrogen bonding.
2. **Sharp Peaks Near 2900–3000 cm^{-1} (C-H Stretching):**
   - These vibrations are due to **C-H stretching** in saturated aliphatic chains or aromatic C-H bonds. Peaks in this region are associated with the decyl chain (in 10-MDP) or aromatic hydrogens (in Phenyl-P).
3. **Strong Peaks at 1700–1750 cm^{-1} (C=O Stretching):**
   - A peak in this range indicates the presence of a **carbonyl group (C=O)**. In 10-MDP, this would correspond to the ester carbonyl group in the methacrylate moiety.
4. **Peaks in the Range of 1200–1300 cm^{-1} (P=O Stretching):**
   - This region is characteristic of the phosphate group. The P=O stretching vibration is typically strong and sharp due to its high dipole moment. This is an important signature for compounds containing phosphate groups, such as Phenyl-P or 10-MDP.
5. **Peaks Near 1000–1150 cm^{-1} (P-O Stretching):**
   - These peaks correspond to the P-O single bond stretching vibrations in the phosphate group. They indicate the presence of phosphate esters or hydrogen phosphates.
6. **Fingerprint Region (500–1500 cm^{-1}):**
   - The region between 500–1500 cm^{-1} contains multiple peaks due to bending and stretching vibrations of various bonds, including C-H bending, C-C stretching, and aromatic or aliphatic ring vibrations. For aromatic compounds, out-of-plane C-H bending may appear in the lower range (600–800 cm^{-1}).

The IR spectrum of 10-MDP reveals key structural features, with intense peaks in the fingerprint region around 1000 cm^{-1} corresponding to P-O-C vibrations and P=O stretching, characteristic of its phosphate group. The C-H stretching vibrations around 3000 cm^{-1} reflect the presence of the alkyl chain and methacrylate group. These features highlight the molecule's adhesive properties, with the phosphate group playing a crucial role in bonding, and the hydrocarbon components contributing to its polymerizable characteristics.

This spectrum serves as a distinct molecular fingerprint for 10-MDP [40].

The IR spectrum of 10-MDP is more active compared to D1 Phenyl-P due to its prominent adhesive properties, characterized by the intense phosphate-related peaks (P=O and P-O-C stretches) around 1000 cm^{-1}, which play a crucial role in bonding with tooth enamel. In contrast, D1 Phenyl-P primarily shows vibrational modes related to aromatic C-H bonds and phosphorus groups, but these do not contribute as significantly to adhesive or polymerizable properties as seen in 10-MDP. Therefore, 10-MDP demonstrates higher activity in terms of functionality for dental applications.

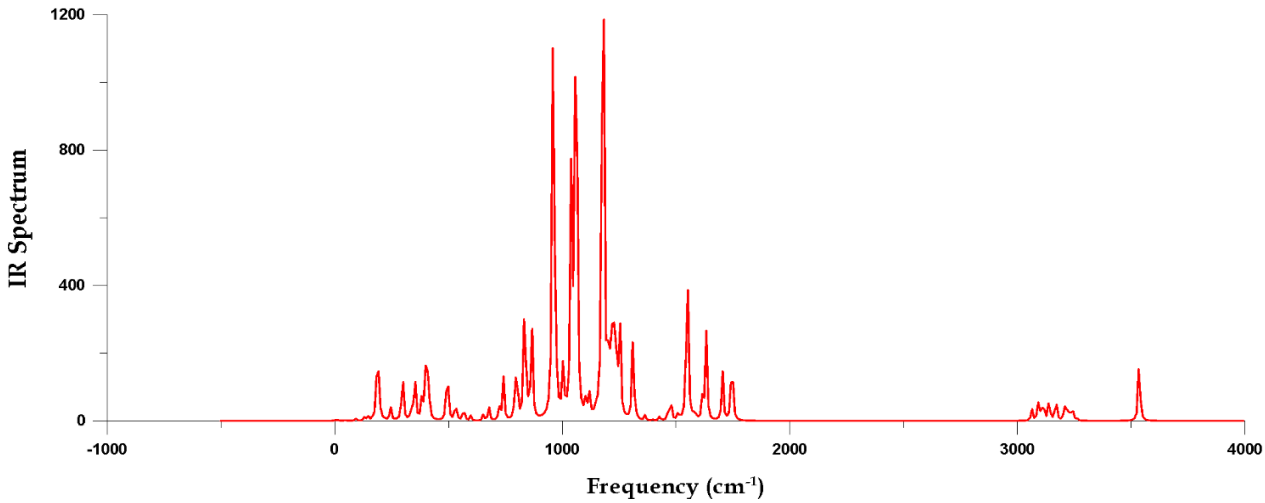

Figure 9. IR spectrum of D1 Phenyl-P [26]

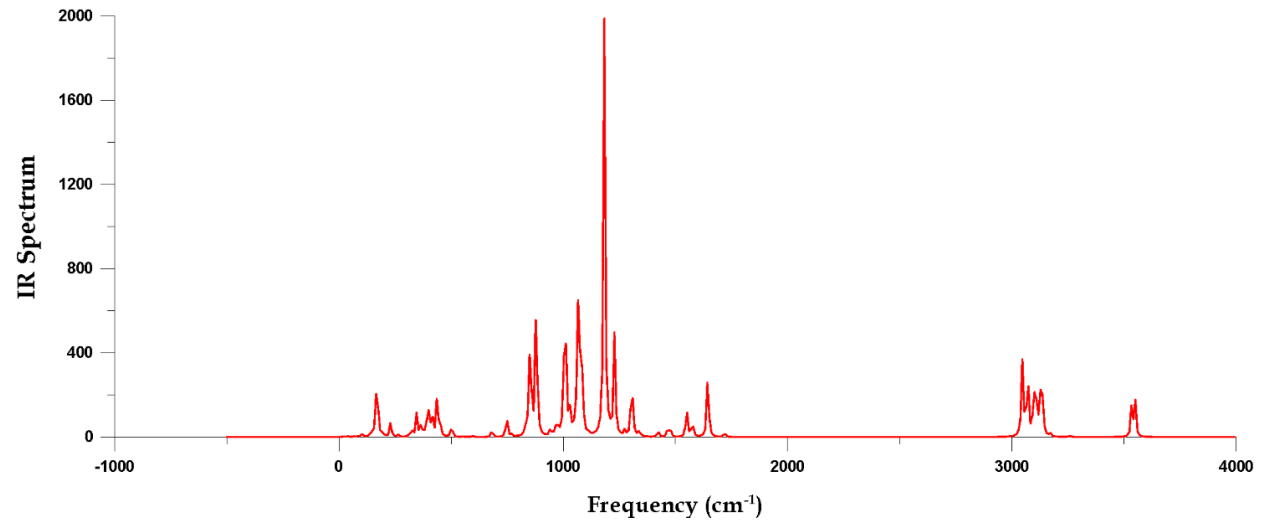

Figure 10. IR spectrum of D2 10 MDP [26]

Figures 8 and 9 illustrate the IR spectra of D1 Phenyl-P and D2 10-MDP, which were obtained using Gaussian View 5.0 software and density functional theory (DFT) with the (6-31G') basis set.

3.5.2 Raman Spectrum (IR) [26]

In Figure 11, the Raman spectrum of D1 Phenyl-P highlights key vibrational modes, with prominent peaks in the fingerprint region (around 1000 cm^{-1}) indicating the presence of C-P, P=O, and aromatic ring vibrations, characteristic of the molecule's phosphorus-containing groups and phenyl ring. The peaks in the 2800–3000 cm^{-1} region are important because they are caused by C-H stretching vibrations from the phenyl group and any alkyl chains. These peaks are quite strong, which means that these functional groups are the most active in the molecule's Raman activity. This gives a thorough vibrational signature that validates the structure and main properties of D1 Phenyl-P [41].

In Figure 12, the Raman spectrum of D2 10-MDP (10-Methacryloyloxydecyl dihydrogen phosphate) reveals key vibrational modes, with prominent peaks in the fingerprint region (around 1000 cm cm^{-1}) corresponding to P-O-C vibrations and P=O stretching, indicative of the phosphate group's presence. Additionally, significant peaks in the (2800-3000 cm^{-1}) range correspond to C-H stretching vibrations, confirming the alkyl chain and methacrylate group. The spectrum provides a clear molecular fingerprint for D2 10-MDP, confirming its structure and highlighting the dominant functional groups that contribute to its chemical behavior [42].

D2 10-MDP is more active compared to D1 Phenyl-P due to the stronger Raman peaks associated with P=O stretching and P-O-C vibrations, which are critical for its adhesive properties in dental applications, whereas D1 Phenyl-P mainly shows activity from aromatic and phosphorus-containing groups that are less involved in bonding interactions.

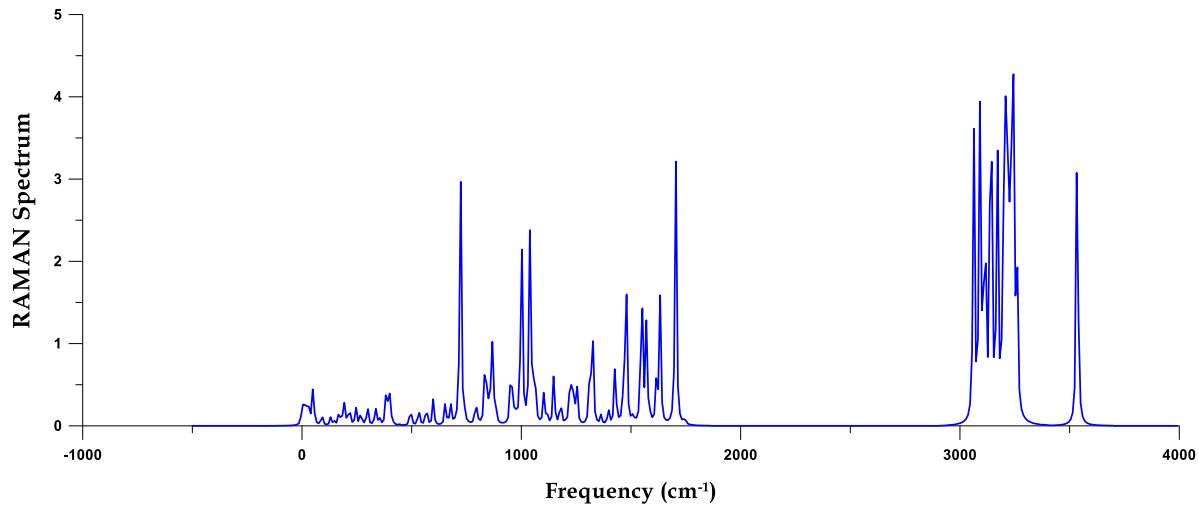

Figure 11. Raman spectrum of D1 Phenyl-P

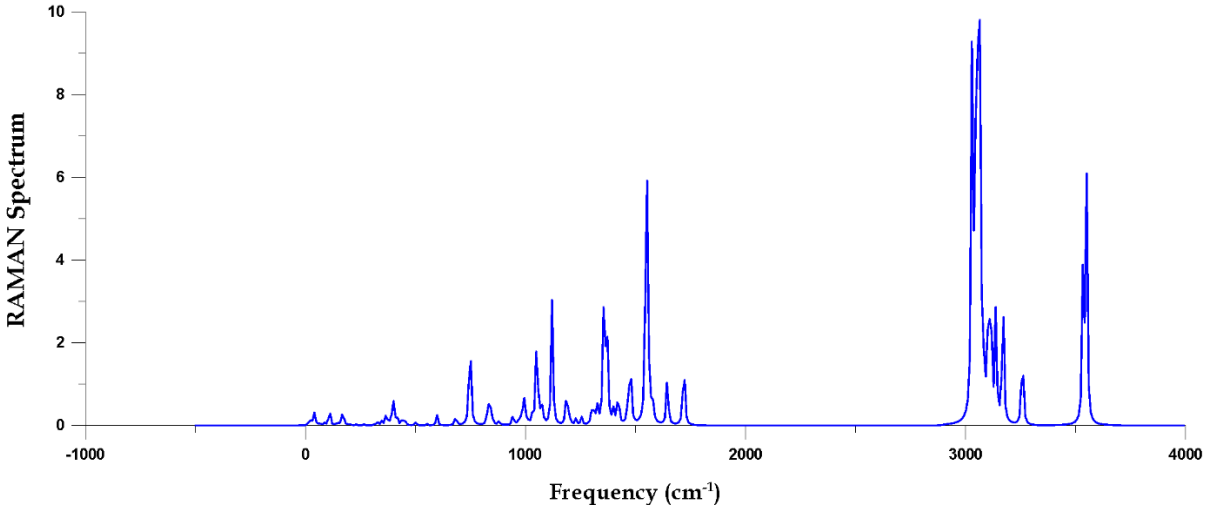

Figure 12. Raman spectrum of D2 10 MDP [26]

3.6 Optical criteria of D1 Phenyl-P, and D2 10 MDP Dental polymers

The figures determined for absorption energy [42] clearly show the absorption behavior. The absorption characteristics of (A) Phenyl-P and (B) D2 10 MDP are shown in Figure 13.

Figure 13 displayed the parameters of absorption of (a) Phenyl-P With an absorption value close to 40,000 cm−1−1, the absorption spectra of Phenyl-P have a pronounced peak at about 13 nm, suggesting substantial UV absorption that is probably caused by π-π* electronic transitions in the phenyl rings. At shorter wavelengths, smaller peaks indicate more structural changes. Absorption quickly decreases after 15 nm and exhibits little interaction with visible and infrared light. Because of this pattern, Phenyl-P is perfect for UV-blocking applications, including coatings or films, since it protects against UV rays while maintaining transparency for visible light. Phenyl-P's aromatic structure plays a role in this activity, which makes it appropriate for industrial and pharmaceutical applications where controlling UV interaction is necessary [43].

Figure 13 showed the absorption properties of (b) D2 10 MDP with the absorption properties of D2 10 MDP, The UV band between 80 and 100 nm and exhibits a significant peak in its absorption spectra, with absorption reaching over (40,000 cm^{-1}). This is most likely because of π-π* electronic transitions in the MDP structure. Around 250 nm (about 15,000 cm^{-1}), there is a secondary, less strong peak that could be caused by n-π* transitions involving carbonyl and phosphate groups. The absorption dramatically drops below 300 nm, suggesting little interaction with visible and near-infrared light. Due to these characteristics, D2 10-MDP is extremely sensitive to UV light, making it appropriate for use as a photo initiator in dental adhesives or as a UV-curable material. Its transparency in the visible range permits it to operate without compromising appearance while promoting strong bonding by UV activation [44].

D2 10-MDP is more active than Phenyl-P due to its stronger UV absorption in the 80-100 nm range, making it highly effective as a UV-curable material and photo initiator for dental adhesives, whereas Phenyl-P primarily absorbs in the 13 nm range for UV-blocking applications but has less interaction with UV light compared to D2 10-MDP.

In Figure 14(a), the diagram shows the imaginary part of the optical conductivity for Phenyl-P over a wide range of wavelengths. Initially, there is a negative dip followed by stabilization, indicating complex interactions between the material and electromagnetic fields at shorter wavelengths. After around 2000 nm, the conductivity approaches near-zero values, suggesting that phenol-P has limited polarization effects at longer wavelengths, mostly in the visible and infrared range. Given this trend, there is little interaction with

longer light wavelengths after a strong initial energy storage period [45].

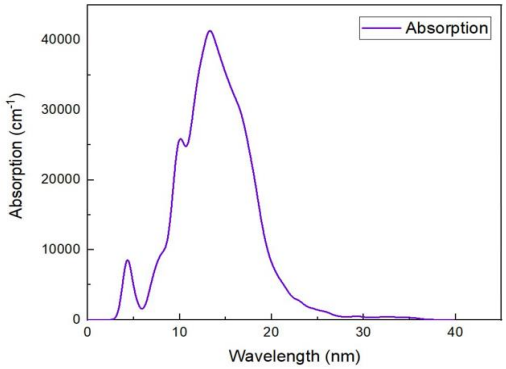

(a) Phenyl-P (D1)

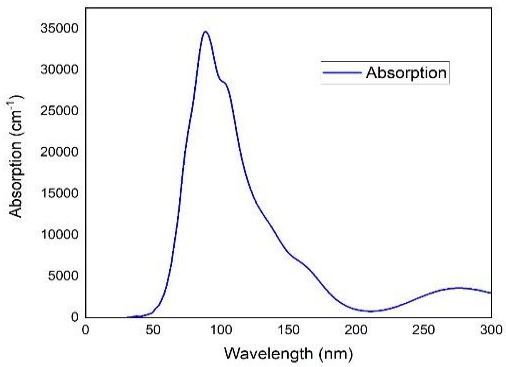

(b) 10 MDP(D2)

Figure 13. The absorption properties of (a) Phenyl-P, (b) D2 10 MDP) [26]

In Figure 14(b), this diagram illustrates the imaginary part of the optical conductivity for 10-MDP plotted against wavelength (nm). It shows a sharp peak near 100 nm, reaching about 0.3 units, which suggests strong polarization effects at short wavelengths. The conductivity then dips into negative values, indicating energy storage in the material, before stabilizing at around 200-300 nm. Beyond 400 nm, the conductivity approaches zero, indicating minimal polarization effects at longer wavelengths. This suggests that 10-MDP interacts more strongly with UV light, with less interaction in the visible ranges [46].

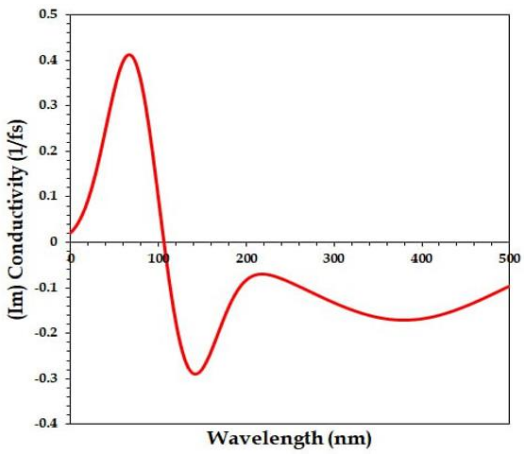

(a) Phenyl-P(D1)

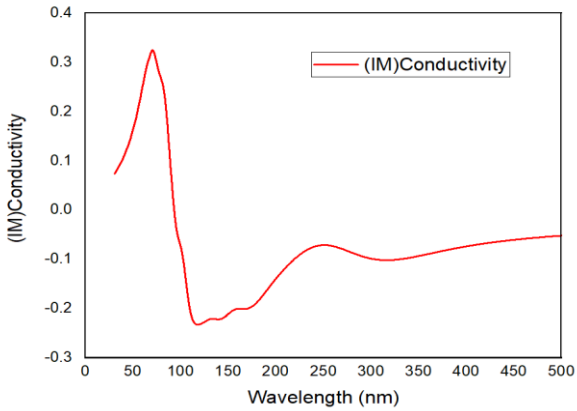

(b) 10 MDP (D2)

Figure 14. The real or actual conductive characteristics of (a) Phenyl-P and (b) D2 10 MDP [26]

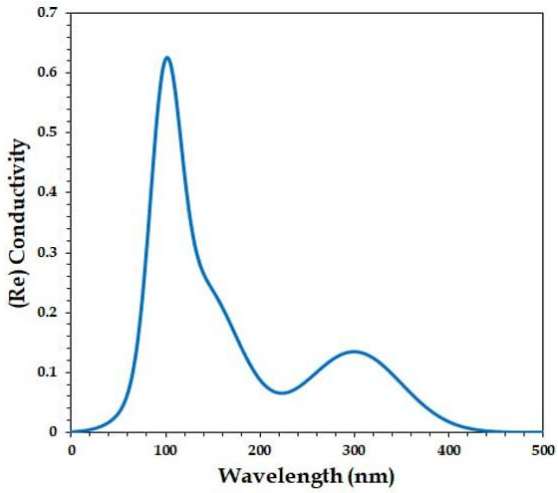

(a) Phenyl-P (D1)

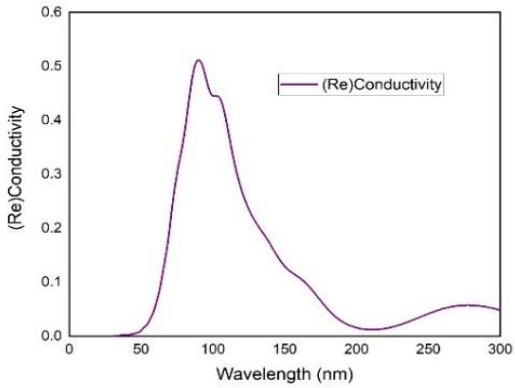

(b) 10 MDP(D2)

Figure 15. The real or actual conductivity characteristics of (a) Phenyl-P, (b) D2 10 MDP) [26]

Figure 15 showed that the real or actual conductivity properties of (a) Phenyl-P, (b) D2 10 MDP).

In Figure 15(a), strong energy dissipation is indicated by D1 Phenyl-P's high conductivity in the UV spectrum, which peaks below 1000 nm. At longer wavelengths, the conductivity almost completely disappears, dropping to almost zero in the visible and infrared ranges. This property makes it appropriate for optoelectronics and UV-curable coatings, and it is good for

UV-activated applications while maintaining transparency in the visible range [47].

In Figure 15(b), the real or actual conductivity of 10-MDP exhibits a prominent peak at 80–100 nm, suggesting a high level of UV light interaction for effective electronic transitions and energy dissipation. The conductivity has negligible interaction with visible and infrared light beyond 400 nm, with a lesser peak occurring at 300 nm. For UV-activated processes such as photopolymerization in dental adhesives, 10-MDP is therefore perfect since it offers strong bonding without compromising transparency in visible light, which is essential for cosmetic dental applications [48, 49].

4. CONCLUSIONS

This research offers an extensive comparison of the quantum chemical and spectroscopic features of D1 Phenyl-P and D2 10-MDP, emphasizing their distinct characteristics and prospective uses. The results obtained using Density functional theory (DFT) with the B3LYP hybrid functional and the G 3-21 basis set reveal distinct differences in their electronic and spectroscopic behaviors, which can be directly linked to their molecular structures and functionalities.

D1 Phenyl-P demonstrates a higher ionization potential and electron affinity, reflecting its greater stability in retaining electrons. This increased chemical hardness makes D1 more resistant to structural deformation, which is a desirable property for applications requiring high durability and stability. However, its lower electronic chemical potential indicates reduced reactivity compared to D2.

In contrast, D2 10-MDP shows higher electronic chemical potential, indicating greater reactivity and a tendency to participate in chemical interactions. Its lower chemical hardness makes it more pliable and reactive, properties that align well with its role as an adhesive agent. Spectroscopic analysis further supports this, with D2 exhibiting stronger P=O and P-O-C vibrations in the IR and Raman spectra, which are critical for its adhesive qualities and interactions with substrates such as hydroxyapatite.

The study also highlights the differences in UV absorption between the two compounds. D2 10-MDP's greater UV absorption in the 80–100 nm region makes it a preferred candidate for UV-curable applications, where efficient UV absorption is crucial for rapid curing and polymerization processes. This property underscores its importance in fields like dental materials and other adhesive technologies.

In summary, D1 Phenyl-P and D2 10-MDP possess complementary properties that make them suitable for distinct applications. D1 is ideal for applications demanding stability and resistance to deformation, whereas D2, with its higher reactivity and superior adhesive qualities, is more suited for environments requiring flexibility, reactivity, and efficient UV-curable performance. The study's findings provide valuable insights into the design and optimization of polymeric fillers for specific functional applications.

REFERENCES

[1] Pan, L., Cai, B. (2023). Phosphate-solubilizing bacteria: advances in their physiology, molecular mechanisms and microbial community effects. Microorganisms, 11(12): 2904. https://doi.org/10.3390/microorganisms11122904

[2] Zhang, Y., Chen, F.S., Wu, X.Q., Luan, F.G., Zhang, L.P., Fang, X.M., Ye, J.R. (2018). Isolation and characterization of two phosphate-solubilizing fungi from rhizosphere soil of moso bamboo and their functional capacities when exposed to different phosphorus sources and pH environments. PloS One, 13(7): e0199625. https://doi.org/10.1371/journal.pone.0199625

[3] Islam, M.K., Sano, A., Majumder, M.S.I., Hossain, M.A., Sakagami, J.I. (2019). Isolation and molecular characterization of phosphate solubilizing filamentous fungi from subtropical soils in Okinawa. Applied Ecology & Environmental Research, 17(4): 9145-9157. https://doi.org/https://doi.org/10.15666/aeer/1704_91459157

[4] Ghosh, A. (2023). Solubilization of soil phosphorus using rice residues and phosphorus solubilizing microorganisms. [Doctoral Dissertation] Division of Soil Science and Agricultural Chemistry ICAR-Indian Agricultural Research Institute, New Delhi.

[5] El Hallal, H. (2019). Introduction To Laser Applications in Dental Treatments. Dental News.

[6] Whelton, H.P., Spencer, A.J., Do, L.G., Rugg-Gunn, A.J. (2019). Fluoride revolution and dental caries: Evolution of policies for global use. Journal of Dental Research, 98(8): 837-846. https://doi.org/10.1177/0022034519843495

[7] Alaarage, W.K., Nasria, A.H.A., Hussein, T.A., Abbood, H.I. (2024). Investigation of the electronic and optical properties of bilayer CdS as a gas sensor: First-principles calculations. RSC Advances, 14(9): 5994-6005. https://doi.org/10.1039/D3RA08741G

[8] Phin, N., Parry-Ford, F., Harrison, T., Stagg, H.R., Zhang, N., Kumar, K., Abubakar, I. (2014). Epidemiology and clinical management of Legionnaires' disease. The Lancet Infectious Diseases, 14(10): 1011-1021. https://doi.org/ 10.1016/S1473-3099(14)70713-3

[9] Banerjee, A., Watson, T.F., Kidd, E.A.M. (2000). Dentine caries: Take it or leave it? Dental Update, 27(6): 272-276. https://doi.org/ 10.12968/denu.2000.27.6.272

[10] Martens, L.C. (2011). Laser physics and a review of laser applications in dentistry for children. European Archives of Paediatric Dentistry, 12(2): 61-67. https://doi.org/10.1007/BF03262781

[11] Wang, J.H., Yang, K., Zhang, B.Z., Zhou, Z.F., Wang, Z.R., Ge, X., Wang, X.J. (2020). Effects of Er: YAG laser pre-treatment on dentin structure and bonding strength of primary teeth: An in vitro study. BMC Oral Health, 20: 316. https://doi.org/10.1186/s12903-020-01315-z

[12] Alviri, V.M., Asem, M.M., Nikbin, A. (2018). Practical assessment of mathematical methods for treatment of tooth cavities using laser based approach. In 2018 IEEE 9th Annual Information Technology, Electronics and Mobile Communication Conference (IEMCON), Vancouver, BC, Canada, pp. 1380-1390. https://doi.org/10.1109/IEMCON.2018.8614872

[13] Shan, X., Miao, Y., Xu, J., Zhang, Q., Gao, X. (2021). Property of high-order Hermite-Gauss beam generated by self-excitation He-Ne laser with intracavity modulator. Optik, 241: 166927. https://doi.org/10.1016/j.ijleo.2021.166927

[14] Müllejans, R., Eyrich, G., Raab, W.H.M., Frentzen, M. (2002). Cavity preparation using a superpulsed 9.6-μm

CO_2 laser-A histological investigation. Lasers in Surgery and Medicine, 30(5): 331-336. https://doi.org/10.1002/lsm.10063
[15] Young, D.C. (2001). A practical guide for applying techniques to real-world problems. Computational Chemistry, New York, 9: 390. https://doi.org/10.1002/0471220655
[16] Mohammad, R.K., Nowfal, S.H., Al-Seady, M.A., Abduljalild, H.M. (2022). Investigation ability of single walled carbon nanotubes to detection toxic gases utilizing DFT Calculations. Egyptian Journal of Chemistry, 65(6): 89-98. https://doi.org/10.21608/EJCHEM.2021.87777.4232
[17] George, D.V. (1972). Principles of Quantum Chemistry. Pergamon.
[18] de Souza, G.L. (2022). Reducing undesirable products: Computational chemistry guiding the experiments. In Green Chemistry and Computational Chemistry, 2022: 245-262. https://doi.org/10.1016/B978-0-12-819879-7.00021-0
[19] Rogalski, A. (2002). Infrared detectors: An overview. Infrared Physics & Technology, 43(3-5): 187-210.
[20] Hussein, T.A., Shiltagh, N.M., Alaarage, W.K., Abbas, R.R., Jawad, R.A., Nasria, A.H.A. (2023). Electronic and optical properties of the BN bilayer as gas sensor for CO2, SO2, and NO2 molecules: A DFT study. Results in Chemistry, 5: 100978. https://doi.org/10.1016/j.rechem.2023.100978
[21] Smith, R., Thomson, R.M. (1978). Computer Modeling of Gas Lasers. Springer New York, NY. https://doi.org/10.1007/978-1-4757-0641-3
[22] Ghani, B.A. (2005). TEA CO_2 laser simulator: A software tool to predict the output pulse characteristics of TEA CO_2 laser. Computer physics communications, 171(2): 93-106. https://doi.org/10.1016/j.cpc.2005.05.007
[23] Soukieh, M., Ghani, B.A., Hammadi, M. (1998). Mathematical modeling of CO_2 TEA laser. Optics & Laser Technology, 30(8): 451–457. https://doi.org/10.1016/s0030-3992(98)00077-2
[24] Wang, T.J., Gao, J.Y., He, Q.Y., Ma, T., Jiang, Y., Kang, Z.H. (2005). Analysis of the dynamics of a mechanical Q-switched CO_2 laser: Six-temperature model. Journal of Applied Physics, 98(7): 073102. https://doi.org/10.1063/1.2084307
[25] Itte, P., Amshumali, M.K., Pasha, M. (2017). Molecular modeling, geometry optimization and characterization of bimetallic complexes derived from s-indacene. Universal Journal of Chemistry, 5(3): 48-57. https://doi.org/10.13189/ujc.2017.050302
[26] Hameed, S., Abdul-Wahid, S. (2025). CO_2 laser applications for sustainable healthcare: Reducing environmental impact in dental enamel cutting. In E3S Web of Conferences, 614: 04024. EDP Sciences. https://doi.org/10.1051/e3sconf/202561404024
[27] Harito, C., Bavykin, D.V., Yuliarto, B., Dipojono, H.K., Walsh, F.C. (2019). Polymer nanocomposites having a high filler content: Synthesis, structures, properties, and applications. Nanoscale, 11(11): 4653-4682. https://doi.org/10.1039/C9NR00117D
[28] Kim, B.G., Ma, X., Chen, C., Ie, Y., Coir, E.W., Hashemi, H., Kim, J. (2013). Energy level modulation of HOMO, LUMO, and band-gap in conjugated polymers for organic photovoltaic applications. Advanced Functional Materials, 23(4): 439-445. https://doi.org/10.1002/adfm.201201385
[29] Alaarage, W.K., Abo Nasria, A.H., Abdulhussein, H.A. (2023). Computational analysis of CdS monolayer nanosheets for gas-sensing applications. The European Physical Journal B, 96(10): 134. https://doi.org/10.1140/epjb/s10051-023-00601-3
[30] Montalti, M., Credi, A., Prodi, L., Gandolfi, M.T. (2006). Handbook of photochemistry. CRC Press. https://doi.org/10.1201/9781420015195
[31] Bandyopadhyay, D. (2012). Chemisorptions effect of oxygen on the geometries, electronic and magnetic properties of small size Ni n (n= 1-6) clusters. Journal of Molecular Modeling, 18: 737-749. https://doi.org/10.1007/s00894-011-1090-8
[32] Carter, E.A., Rossky, P.J. (2006). Computational and theoretical chemistry. Accounts of Chemical Research, 39(2): 71-72. https://doi.org/10.1021/ar050190o
[33] Sadasivam, K., Kumaresan, R. (2011). Theoretical investigation on the antioxidant behavior of chrysoeriol and hispidulin flavonoid compounds–A DFT study. Computational and Theoretical Chemistry, 963(1): 227-235. https://doi.org/10.1016/j.comptc.2010.10.025
[34] Pasquini, C. (2003). Near infrared spectroscopy: fundamentals, practical aspects and analytical applications. Journal of the Brazilian Chemical Society, 14: 198-219. https://doi.org/10.1590/S0103-50532003000200006
[35] Alaarage, W.K., Nasria, A.H.A., Alkhayatt, A.H.O. (2023). A DFT investigation of an InP bilayer: a potential gas sensor with promising adsorption and optical response. Computational and Theoretical Chemistry, 1227: 114223. https://doi.org/10.1016/j.comptc.2023.114223
[36] Liang, G.C., Ghosh, A.W., Paulsson, M., Datta, S. (2004). Electrostatic potential profiles of molecular conductors. Physical Review B, 69(11): 115302. https://doi.org/10.1103/PhysRevB.69.115302
[37] Roh, J., Shin, H., Hong, M.H. (2020). Characteristics of 10-methacryloyloxidecyl dihydrogen phosphate monomer in self-etching two-bottled dental adhesive system: Comparison with commercial products. Materials, 13(16): 3553. https://doi.org/10.3390/ma13163553
[38] Gateaa, Z.A., Abo Nasria, A., Abojassim, A.A. (2022). Adsorption of gas molecules on (BN) monolayer as potential SO, SO_2 NO, and NO_2 gases sensor: A DFT study. Egyptian Journal of Chemistry, 65(3): 363-374. https://doi.org/10.21608/ejchem.2021.92587.4380
[39] Furtado, P.R.P., Savanhago, R.M., Castro, N., Gariani, R. A., Meier, M.M. (2024). Synthesis and characterization of the dental adhesive monomer 10-MDP. Dental Materials, 40(11): 2000-2007. https://doi.org/10.1016/j.dental.2024.09.009
[40] Copeland, T., Shea, M.P., Milliken, M.C., Smith, R.C., Protasiewicz, J.D., Simpson, M.C. (2003). Raman excitation profile of a sterically protected diphosphene [ArP PAr]. Analytica chimica acta, 496(1-2): 155-163. https://doi.org/10.1016/S0003-2670(03)00996-6
[41] De-Paula, D.M., Loguercio, A.D., Reis, A., Frota, N.M., Melo, R., Yoshihara, K., Feitosa, V.P. (2017). Micro-raman vibrational identification of 10-MDP bond to zirconia and shear bond strength analysis. BioMed Research International, 2017(1): 8756396.

https://doi.org/10.1155/2017/8756396
[42] Shao, Y., Yin, G.Z., Ren, X., Zhang, X., Wang, J., Guo, K., Sun, B. (2017). Engineering π–π interactions for enhanced photoluminescent properties: Unique discrete dimeric packing of perylene diimides. RSC Advances, 7(11): 6530-6537. https://doi.org/10.1039/C6RA28147H
[43] Hussein, T.A., Alaarage, W.K., Abdulhussein, H.A., Seriani, N., Nasria, A.H.A. (2023). Ga-doped AlN monolayer nano-sheets as promising materials for environmental sensing applications. Computational and Theoretical Chemistry, 1223: 114086. https://doi.org/10.1016/j.comptc.2023.114086
[44] Chen, J., Lin, H. Y., Ji, X., Zhao, H., Sun, B., Wang, C. L., Zhu, M. (2021). Host–guest chemistry of giant molecular shape amphiphiles based on POSS–PDI conjugates. Nanoscale, 13(7): 4295-4300. https://doi.org/10.1039/D0NR08934F
[45] Gonciarz, A., Pich, R., Bogdanowicz, K.A., Jewloszewicz, B., Przybył, W., Dysz, K., Januszko, A. (2019). UV–Vis Absorption Properties of New Aromatic Imines and Their Compositions with Poly ({4, 8-bis [(2-Ethylhexyl) oxy] Benzo [1, 2-b: 4, 5-b'] Dithiophene-2, 6-diyl}{3-Fluoro-2-[(2-Ethylhexyl) Carbonyl] Thieno [3, 4-b] Thiophenediyl}). Materials, 12(24): 4191. https://doi.org/10.3390/ma12244191
[46] Lacroix, P.G., Nakatani, K. (1997). Multiproperty molecular materials combining conductivity and second-order optical nonlinearities. Advanced Materials, 9(14): 1105-1108. https://doi.org/10.1002/adma.19970091409
[47] Wu, Q., He, T., Zhang, Y., Zhang, J., Wang, Z., Liu, Y., Ran, F. (2021). Cyclic stability of supercapacitors: Materials, energy storage mechanism, test methods, and device. Journal of Materials Chemistry A, 9(43): 24094-24147. https://doi.org/10.1039/D1TA06815F
[48] Oweis, Y.G. (2020). Surface Chemical Modification of Dental Materials. McGill University (Canada).
[49] Patra, A., Chandaluri, C.G., Radhakrishnan, T.P. (2012). Optical materials based on molecular nanoparticles. Nanoscale, 4(2): 343-359. https://doi.org/10.1039/C1NR11313E